# Active Suspension System Based on Linear Switched Reluctance Actuator and Control Schemes

Jiongkang Lin, Ka Wai Eric Cheng, *Senior Member, IEEE*, Zhu Zhang, *Student Member, IEEE*, Norbert C. Cheung, *Senior Member, IEEE*, Xiangdang Xue, *Member, IEEE*, and Tsz Wang Ng

***Abstract*—In this paper, an active suspension system utilizing a low-cost high-performance linear switched reluctance actuator with proportional-derivative (PD) control is presented. With the tracking differentiator (TD) calculating the displacement and its derivatives directly under the presence of noise, velocity and acceleration can be evaluated, and accurate position control can be achieved. Comparison is made between linear and nonlinear PD control methods in terms of various system parameters and road profiles. A nonlinear PD controller with better dynamic responses is evaluated and developed for real-time suspension application. The proposed PD control schemes are simulated, tested, and analyzed to prove its robustness and reliability. Finally, a quarter-car active suspension system prototype is built to demonstrate the effectiveness of the proposed control schemes with experiment results.**

***Index Terms*—Active suspension system, linear switched reluctance actuator (LSRA), nonlinear PD, tracking differentiator (TD).**

## I. Introduction

ACTIVE suspension systems have been investigated and developed for decades. Compared with the passive and active hydraulic suspension system, the active electromagnetic suspension system is more suitable for the electric vehicle due to its simple mechanical construction and fast dynamic response. It can also be used for any vehicle for comfort improvement through better position and acceleration control of the sprung mass part.

Linear permanent-magnet actuators are the most popular type of electric actuator for active suspension system. Martins *et al.* proposed the potential of permanent-magnet actuator for implementing the active suspension system [1] to meet the requirement of "reduced comfort boundary" [2]. The study of an active suspension system with tubular permanent-magnet actuator is attempted in [3] to specify the design constraints for passenger vehicles. The response of a quarter-car active electromagnetic suspension system is presented in [4] with direct drive of linear actuator, which indicated the probability of all electric active suspension systems to reject road disturbance.

High cost, difficult assembly, and maintenance are the main drawbacks of permanent-magnet actuators, particularly due to the rapidly rising cost of rare earth. Linear switched reluctance actuator (LSRA) is a potential alternative for active electromagnetic suspension system due to its simple structure and low cost as well as reliability and high performance [5]. Recently, the LSRA has been investigated and applied in vertical propulsion systems for elevators. Its direct drive control method is developed to overcome the control complexity, and satisfied performance is achieved [6]–[10]. An LSRA with PD control in an electromagnetic active suspension system of automotive application is the first ever developed and presented in this paper.

The main objective of the active suspension system is to minimize or eliminate vibration hazards and isolate the vehicle body from road irregularities. Nowadays, much research work has been done on intelligent control methods and $H_\infty$ control, which enhance the flexibility of active suspension control systems to fulfill the requirements [11]–[14], [15]. Intelligent control methods [11]–[14] are theoretically available and have excellent performance. $H_\infty$ control methods [15] are widely discussed for their robustness of parameter variation and disturbances. However, these methods impose huge calculation burdens to the controller, which are impractical in real-time embedded control systems.

To overcome this drawback in embedded control systems, the PD controller offers a simple and reliable solution [16]. In this paper, a nonlinear PD controller [17]–[19] is developed to enhance the robustness of the embedded control system. Both linear and nonlinear PD control methods are validated in simulation and verified by experiment results.

Meanwhile, vertical displacement, velocity, and acceleration are critical attributes in active suspension system control and hardware implementation. Acquiring velocity parameters using conventional calculations is obstructed by the noisy feedback displacement signal. A novel tracking differentiator (TD) is introduced to track the feedback displacement signal and calculate its velocity directly through the numerical method based on optimal control theory [17], [19].

This paper is organized as follows. A description of the active suspension system and design of the experimental platform are proposed in Section II. Section III shows how the TD calculates the derivative of displacement and how linear and nonlinear PD controls are implemented to generate active forces and

Manuscript received January 18, 2012; revised May 20, 2012, July 31, 2012, and September 20, 2012; accepted September 25, 2012. Date of publication January 4, 2013; date of current version February 12, 2013. This work was supported in part by the Innovation and Technology Fund of Hong Kong and in part by the Hong Kong Automotive Parts and Accessory Systems R&D Centre under Project ITP02509AP. The review of this paper was coordinated by Dr. M. S. Ahmed.

The authors are with the Department of Electrical Engineering, The Hong Kong Polytechnic University, Kowloon, Hong Kong (e-mail: ee.jklin@connect.polyu.hk; eeecheng@polyu.edu.hk; ee.zz@connect.polyu.hk; norbert.cheung@polyu.edu.hk; eexdxue@polyu.edu.hk; eetwng@polyu.edu.hk).

Color versions of one or more of the figures in this paper are available online at http://ieeexplore.ieee.org.

Digital Object Identifier 10.1109/TVT.2012.2222682

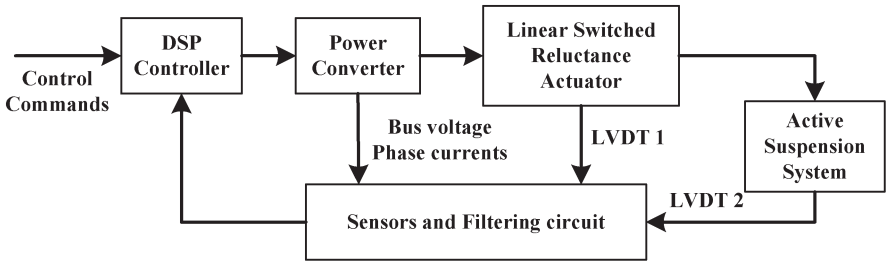


Fig. 1. Block diagram of quarter-car active suspension system.

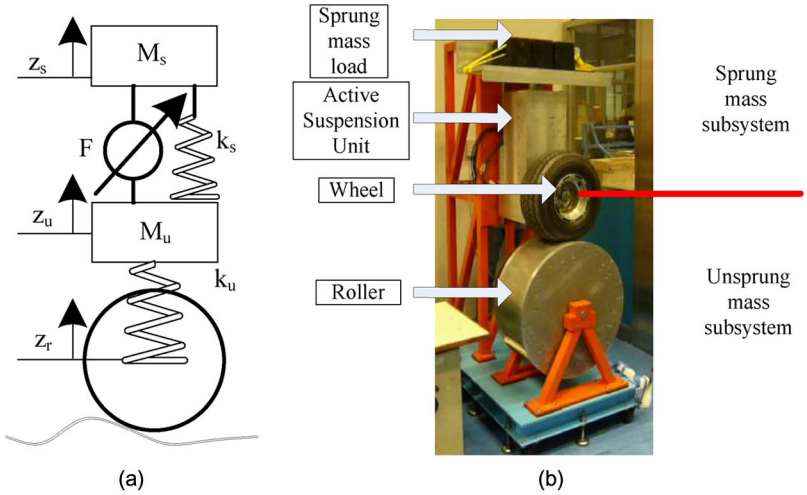


Fig. 2. Configuration of quarter-car active suspension system. (a) Sketch. (b) Prototype.

reject vertical vibrations. Simulation and experiment results that verify the validity of the proposed controllers are demonstrated in Section IV. The conclusion and future development are discussed in Section V.

## II. System Description and Platform Design

### A. Active Suspension System Overview

A block diagram showing a quarter-car active suspension system is given in Fig. 1. A series of commands, such as vertical displacement and limitation of velocity, are input into the control unit. Meanwhile, system status, such as phase currents and position signals, is acquired by sensors and feedback to the DSP controller. Then, the LSRA is turned on and off in sequence through the power converter and generates the required force to sustain the sprung mass subsystem regardless of vertical vibration.

### B. System Configuration

The sketch of the quarter-car active suspension system is described in Fig. 2(a). The active suspension unit is composed of a passive spring and an active linear actuator. They are parallel connected with the aim to 1) sustain the sprung mass subsystems, and 2) reject the road irregularities, which are experienced by the unsprung mass subsystem. The elasticity of the wheel is simply presented by a passive linear spring with large stiffness in Fig. 2(a). In Fig. 2(b), an experimental prototype is set up in the laboratory. The bottom roller is driven by a mover that delivers the vertical vibrations to the wheel to generate man-made road irregularities. Table I lists the symbols used in the active suspension system.

TABLE I
Symbol of Active Suspension System

| Symbol | Quantity |
|---|---|
| $z_s$ | Displacement of sprung mass subsystem |
| $z_u$ | Displacement of unsprung mass subsystem |
| $z_r$ | Road disturbance |
| $F$ | Actuator force |
| $M_s$ | Sprung mass |
| $M_u$ | Unsprung mass |
| $K_s$ | Spring stiffness |
| $K_u$ | Tire stiffness |

### C. LSRA

The proposed LSRA is composed of four identical double-sided actuator modules, as shown in Fig. 3. The stator and translator core are laminated to reduce eddy current losses. Fig. 3(a) shows the configuration of the double-sided module, which is made of four phases with eight pairs of stator poles and eight translator poles. The translator weight is considerably reduced due to the absence of excitation windings and back iron. Moreover, there is no permanent magnet, which is more suitable for harsh environments. A double-sided structure has the advantage of higher force density than a single-sided structure, and four double-sided LSRA modules can be integrated in a more compact configuration as depicted in Fig. 3(b). A

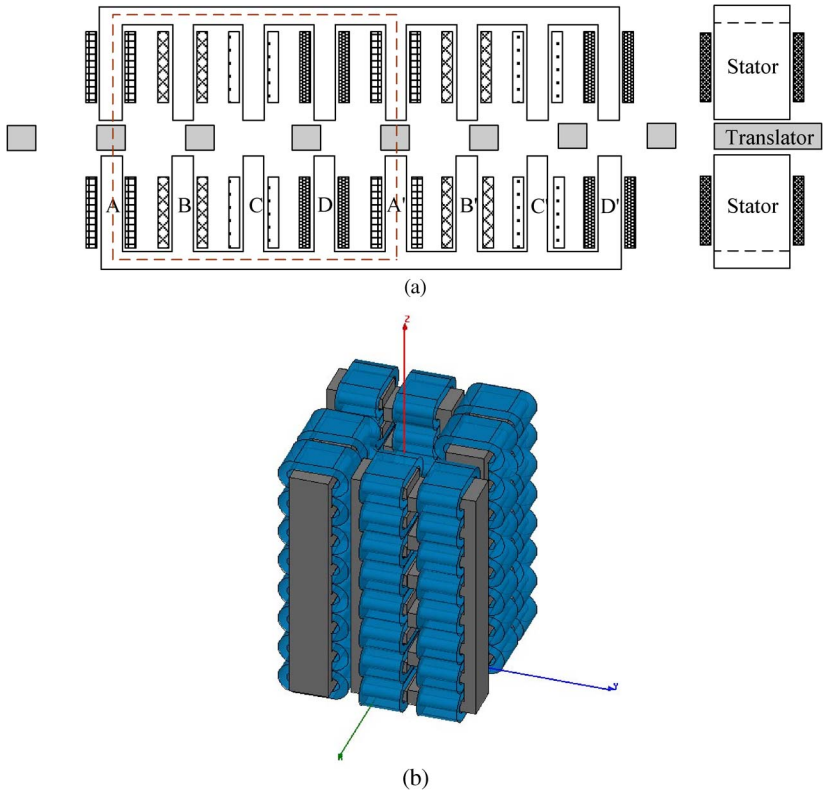


Fig. 3. LSRA model. (a) Configuration of double-sided LSRA module. (b) 3-D FEM model of LSRA.

TABLE II
SPECIFICATION OF LSRA

| Quantity | Value | Quantity | Value |
|---|---|---|---|
| Number of modules | 4 | DC-link voltage | 200 V |
| Number of phases per module | 4 | Nominal current | 10 A |
| Number of stator poles per module | 16 | Peak transient power | 4.8 kW |
| Number of translator poles per module | 8 | Stroke | 96 mm |
| Stator pole pitch | 36 mm | Nominal force | 125 N |
| Translator pole pitch | 48 mm | Peak force | 500 N |
| Stator pole width | 13mm | | |
| Translator pole width | 17 mm | | |
| Stator pole height | 49 mm | | |
| Stator yoke thickness | 13 mm | | |
| Stack length | 43 mm | | |

high propulsion force is provided by four modules in parallel, whereas the lateral forces generated by both sides of the stator are eliminated by force balancing. Moreover, this elimination is helpful for reducing acoustic noise during the operation. Finally, this configuration is easier for heat dissipation due to the good thermal contact of the coil and the actuator frame, which consequently enhances the overload capability of the LSRA.

The force characteristic of the proposed LSRA is calculated by the finite element analysis (FEA) method. Compromise between actuator size and output electromagnetic force has been taken into account in the design procedure of the LSRA. The detailed parameters of the LSRA module are specified in Table II. The peak force of the LSRA is determined as 2000 N to satisfy the requirement of a medium-sized vehicle based on "reduced comfort boundary" [2]. The force characteristic of a double-sided LSRA module shows that positive (upward) and negative (downward) forces are generated symmetrically in a period (48 mm) and varied with positions and currents, as shown in Fig. 4(a). In Fig. 4(b), the derivative of the phase inductance according the position is obtained by the FEA method, which is used to generate current command in the inner current closed-loop control [20]–[23].

The same phases of each module are connected in series, and the converter units can be minimized to reduce the converter cost. In this application, capacitors of large capacitance are connected electrically in parallel with batteries. Thus, the transient energy required by the peak power can be supplied by both the capacitors and the batteries. In addition, the capacitors are used to store the regenerated transient energy from the active suspension.

The actual power consumption for the suspension depends on the road surface. The energy consumed depends on the duration that a vehicle passes through a ramp or any uneven surface.

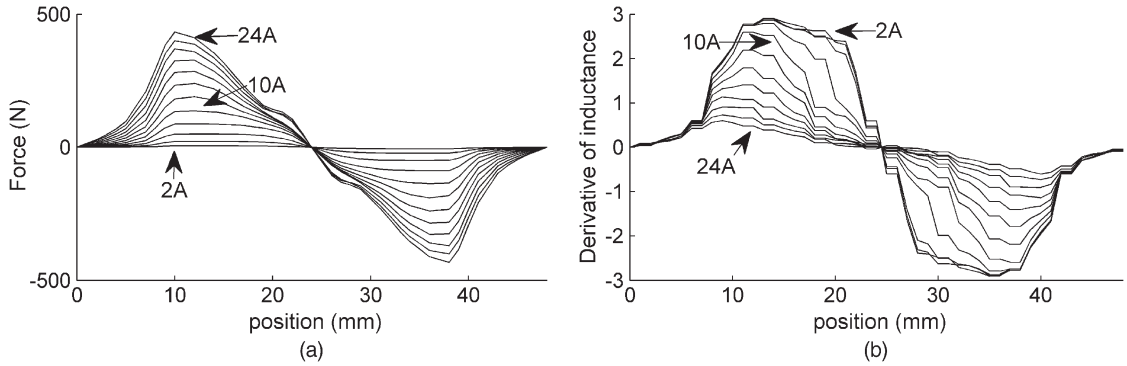


Fig. 4. Characteristic of LSRA module. (a) Force characteristics. (b) Derivative of inductance versus position.

In our laboratory test, the average consumed power is about 350 W. Hence, the total required power for a four-wheel vehicle is 1.4 kW.

### D. Sensors

The active suspension system can be classified as mechanical and electrical systems; therefore, both types of sensors are required in the real-time application. For the mechanical part, an internal linear variable displacement transducer (LVDT) is used to detect the relative position of stator and translator for appropriate conduction. The external LVDT monitors the displacement of the sprung mass subsystem for control purpose. For the electrical part, the voltage sensor is connected in the bus to protect the LSRA from overvoltage; four current sensors are independently installed to each phase to realize the closed-loop implementation.

## III. Linear and Nonlinear PD Control Method With Tracking Differentiator

In this section, the active suspension system is modeled linearly to describe the motion relationship, and then a reduced model is extracted for control purpose. The TD is introduced in this system to acquire and smoothen both vertical displacement and its velocity of sprung mass subsystem. Linear/nonlinear PD control is used to generate the required electric force and then suppresses the vertical vibration. The control schematic of the active suspension system is presented in Fig. 5(a), whereas the direct force drive of the LSRA is shown in Fig. 5(b).

### A. Model of Active Suspension System

The active suspension system described in Fig. 2 can be modeled as follows by applying the force balancing principle:

$$\begin{cases} M_s\ddot{z}_s = -K_s(z_s - z_u) - C_s(\dot{z}_s - \dot{z}_u) + F \\ M_u\ddot{z}_u = K_s(z_s - z_u) + C_s(\dot{z}_s - \dot{z}_u) - F - K_u(z_u - z_r) \end{cases} \tag{1}$$

where $C_s$ is equivalent damper coefficient due to friction in the active suspension system.

The control objective is to keep the sprung mass subsystem stable, whose position and velocity are chosen as state variables, and the position and velocity of the unsprung mass

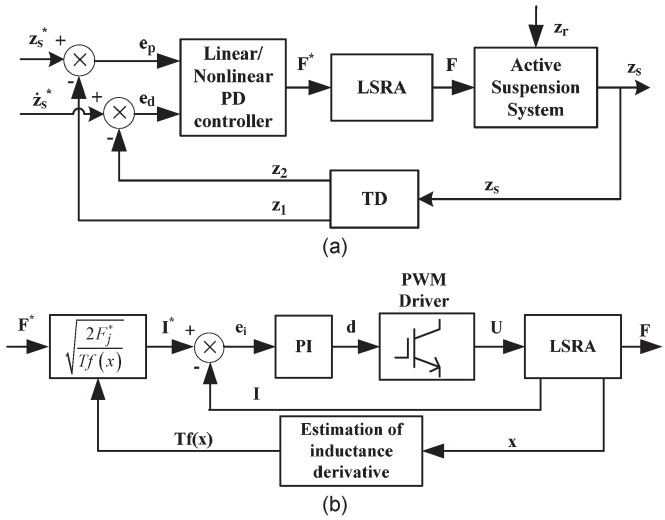


Fig. 5. Schematic of active electromagnetic suspension system. (a) Control of active suspension system. (b) Direct force drive of LSRA.

system can be regarded as external disturbances. Letting $x_1 = z_s$, $x_2 = \dot{z}_s$, $d_u = [z_u \quad \dot{z}_u]^T$, the model can be rewritten as

$$\begin{bmatrix} \dot{x}_1 \\ \dot{x}_2 \end{bmatrix} = \begin{bmatrix} 0 & 1 \\ -K_s/M_s & -C_s/M_s \end{bmatrix} \begin{bmatrix} x_1 \\ x_2 \end{bmatrix} + \begin{bmatrix} 0 \\ 1/M_s \end{bmatrix} F + \begin{bmatrix} 0 & 0 \\ K_s/M_s & C_s/M_s \end{bmatrix} d_u. \tag{2}$$

### B. Direct Drive of LSRA

Voltage balancing of the LSRA is presented as

$$u_j = R_s i_j + \frac{d\lambda_j}{dt} = R_s i_j + L_j \frac{di_j}{dt} + v i_j \frac{dL_j}{dx}, \quad j = a, b, c, d \tag{3}$$

where $u_j$ and $i_j$ are the phase voltage and phase current, $R_s$ and $L_j$ are the related resistance and inductance, $\lambda_j = L_j i_j$ is phase flux linkage, $x$ is the translator displacement, while $v = \dot{x}$ is its velocity.

The phase current equation is obtained from (3) as

$$\frac{di_j}{dt} = -\frac{R_s}{L_j} i_j - \frac{v}{L_j} \frac{dL_j}{dx} i_j + \frac{1}{L_j} u_j, \quad j = a, b, c, d \tag{4}$$

where the phase inductance is a function of position and phase current: $L_j = L_j(x, \quad i_j)$.

The output force of the LSRA is the sum of phase forces; the phase force is a function of the current and the derivative of the inductance according the position. The relationship can be written as

$$F = \sum_j F_j,\ F_j = \frac{1}{2}\left(\frac{dL_j}{dx}\right) i_j^2, \quad j = a, b, c, d \tag{5}$$

where $F_j$ is the phase electrical force, and $F$ is the total electrical force.

Phase overlapping control is not adopted in this application due to the small high force intersecting area implied by Fig. 4(a). The inductance and its derivative of LSRA are highly nonlinear and varied with phase currents and position, as shown in Fig. 4(b). Several methods are attempted to describe the complicated behavior of phase inductance variation, such as numerical and analytical functions [20]–[23]. A lookup table is a convenient tool to depict the inductance change rate; the only requirement is to pre-obtain a large amount of data by measurement or FEA. To overcome this drawback, a simple and easy method with least data is tried to be developed in this paper to reduce the computation burden. A force factor function $Tf(x)$ is introduced here to estimate the value of the inductance change rate, which is based on the FEA curve of phase inductance at nominal current. The difference between the force factor $Tf(x)$ and the real derivative of the phase inductance $(dL/dx)$ can be compensated by the closed-loop current controller [6]. The force factor can be chosen in many forms based on the maximum value of derivative of inductance, which appears around the center of the phase conducting interval; one simple quadratic form is

$$Tf(x) = \left.\frac{dL_j}{dx}\right|_{\max}\left(1 - \frac{(x - x_{cj})^2}{36} t_k\right), \quad 0 < t_k \le 1 \tag{6}$$

where $(dL_j/dx)|_{\max}$ is the maximum inductance change rate at nominal current, $x_{cj}$ are the centers of phase conducting zones that satisfy $|x - x_{cj}| \le 6$, and $t_k$ is the ratio between the minimum and maximum value of change rate curve and set to be 0.2 in this paper.

The current command is estimated as

$$i_j^* = \sqrt{\frac{2F_j^*}{Tf(x)}}. \tag{7}$$

The control schematic is shown in Fig. 5(b); a closed-loop current control with proportional-integral control is used to drive the LSRA and provide high force to stabilize the active suspension system.

### C. TD

Nonlinear TD [17], [24] is an effective way to solve the practical acquisition of a differential signal for real-time application. The discrete signals $r_1$ and $r_2$ of TD are the traces of the reference input $r$ following an optimal path

$$\begin{cases} r_1(k+1) = r_1(k) + hr_2(k) \\ r_2(k+1) = r_2(k) + hfst\left(r_1(k) - r(k), r_2(k), \upsilon, ch\right) \end{cases} \tag{8}$$

where $h$ is the sampling step, $\upsilon$ is the tracking velocity factor for signal tracking, and $c$ is the filtering factor to reject stochastic noise. The update function $fst(p_1, p_2, \upsilon, H)$ is of the form

$$fst(p_1, p_2, \upsilon, H) = \begin{cases} -\upsilon \text{sign}(a), & |a| > d \\ -\upsilon \frac{a}{d}, & |a| \le d \end{cases} \tag{9}$$

with

$$a = \begin{cases} p_2 + \frac{b-d}{2}\text{sign}(\gamma), |\gamma| > d^2 \\ p_2 + \frac{\gamma}{d}, |\gamma| \le d^2 \end{cases}$$

$$d = \upsilon H,\ \gamma = \upsilon p_1 + dp_2,\ b = \sqrt{d^2 + 8|\gamma|}.$$

For the active suspension system, the external LVDT signal $z_s$ is acquitted to the controller with sensor white noise, and the first step is to smooth the signal and calculate vertical velocity by TD. The smoothed displacement signal $z_1$ and the vertical velocity $z_2$ are derived from

$$\begin{cases} z_1(k+1) = z_1(k) + hz_2(k) \\ z_2(k+1) = z_2(k) + hfst\left(z_1(k) - z_s(k), z_2(k), \upsilon, ch\right). \end{cases} \tag{10}$$

The performance of nonlinear TD mainly depends on $\upsilon$ and $c$. A large $\upsilon$ is beneficial for fast transition and tracking, and a large $c$ is helpful to reject stochastic sensor noise. However, improper choice of parameters will deteriorate the system performance. A too large $\upsilon$ causes chattering of the output signals, particularly the derivative of the reference signal. A too large $c$ will delay the response of the system. Moreover, there is a tradeoff between tracking and filtering. In [17], a general principle of selecting parameters is stated as follows: for the reference signal with maximum noise of 0.01, $\upsilon \in [2.5,\ 50]$; for the reference signal with larger noise, $\upsilon$ will be increased to obtain good tracking performance, whereas the differential signal will be deteriorated.

In this application, the filtering factor is fixed first. As mentioned above, a large filtering factor is required to cancel the sensor noise injected by components and motor drive. Then, a large velocity factor is used for the simulation test. Several combinations of $(\upsilon,\ c)$ are tested, i.e., (250, 10), (200, 10), (200, 5), and (150, 5). Based on the simulation results, (200, 10) is selected as the best parameters of TD. To demonstrate the effect of nonlinear TD, tracking of sinusoidal road with measured noise is shown. The reference of TD is 0.05 m with a frequency of 3.33 Hz and 0.001 m white noise. The tracking of reference is achieved as shown in Fig. 6, and the velocity is obtained simultaneously, which is unavailable in conventional calculation. Furthermore, the acceleration is easy to obtain through tracking the output velocity by one more TD.

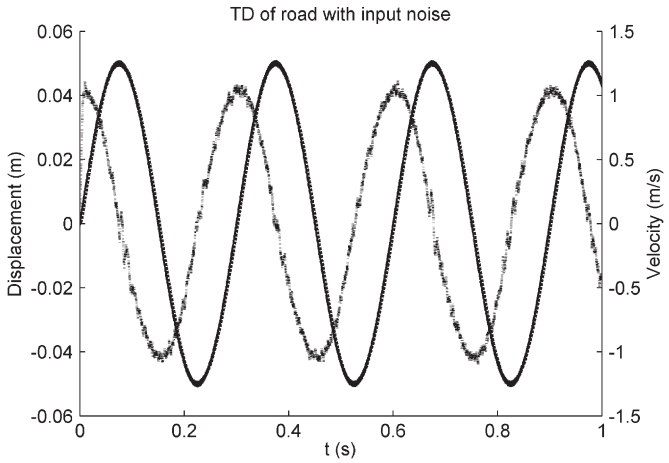


Fig. 6. TD of sinusoidal road profile ($v = 200, c = 10, h = 0.00025$).

### D. PD Controller

The feedback displacement and its velocity can be obtained through TD, as previously discussed . The reference commands of the active suspension system are referred to as zero displacement and zero velocity, i.e., $z_s^* = 0$ and $\dot{z}_s^* = 0$; hence, the input errors are classified into proportional error $e_p = z_s^* - z_1 = -z_1$ and derivative error $e_d = \dot{z}_s^* - z_2 = -z_2$.

The conventional linear PD controller is of the form

$$F^* = k_{lp}e_p + k_{ld}e_d \tag{11}$$

where $k_{lp}$ and $k_{ld}$ are the proportional and derivative gains.

The PD controller of (11) is composed of a proportional item related to displacement and a derivative item related to velocity. The derivative gain $k_{ld}$ should be determined first to suppress the vertical vibration due to road disturbance; the proportional gain $k_{lp}$ is tuned later to smooth the response of the system.

The linear PD controller is simple and satisfied enough for implementation. The possible drawback is the linear fixed gain between output and errors. A nonlinear feedback error strategy is helpful to solve that conflict [17]–[19]. The form of nonlinear PD control law is similar to classical PD control and can be synthesized as

$$F^* = k_{np}(\cdot)e_p + k_{nd}(\cdot)e_d \tag{12}$$

where $k_{np}(\cdot)$ and $k_{nd}(\cdot)$ are error-dependent time-varying nonlinear gains.

The purpose of employing nonlinear PD controller is to reduce the rise time of small error and to enhance the robustness of large error, which is mainly due to the increasing amplitude of road disturbance. One possible nonlinear PD controller is of the form

$$F^* = k_p p(e_p,\ \delta_p,\ \alpha_{p1},\ \alpha_{p2}) + k_d p(e_d,\ \delta_d,\ \alpha_{d1},\ \alpha_{d2}) \tag{13}$$

where $k_p$ and $k_d$ are the proportional and derivative gains to be determined, $\delta_p$ and $\delta_d$ are error set points, and $\alpha_{p1}$, $\alpha_{p2}$, $\alpha_{d1}$, and $\alpha_{d2}$ are converging factors.

The nonlinear error function $p(e,\ \delta,\ \alpha_1,\ \alpha_2)$ is denoted as

$$p(e,\ \delta,\ \alpha_1,\ \alpha_2) = \begin{cases} |e/\delta|^{\alpha_1}\text{sign}(e), |e| > \delta \\ |e/\delta|^{\alpha_2}\text{sign}(e), |e| \le \delta \end{cases}, \delta > 0. \tag{14}$$

Substituting (14) into (13), the nonlinear time-varying gains are obtained as

$$k_{np}(\cdot) = \begin{cases} k_p|e_p|^{\alpha_{p1}-1}\delta^{-\alpha_{p1}}, |e| > \delta_p \\ k_p|e_p|^{\alpha_{p2}-1}\delta^{-\alpha_{p2}}, |e| \le \delta_p, \delta_p > 0 \end{cases}$$

$$k_{nd}(\cdot) = \begin{cases} k_d|e_d|^{\alpha_{d1}-1}\delta_d^{-\alpha_{d1}}, |e| > \delta_d \\ k_d|e_d|^{\alpha_{d2}-1}\delta_d^{-\alpha_{d2}}, |e| \le \delta_d, \delta_d > 0 \end{cases}. \tag{15}$$

The analysis of linear and nonlinear PD is further examined in the following.

*1) Main Difference Between Linear PD and Nonlinear PD Controllers:* From (15), the nonlinear PD controller is with time-varying gains, whereas the gains of linear PD are fixed, which provides a more flexible choice for the closed-loop controlled system and enhances the system performance [17], [18]. It is assumed that the linear and nonlinear PD controllers have identical output at their error set points, such as the proportional terms in both controllers have the same force at $|e| = \delta = 0.1$. The outputs of the nonlinear PD controller related to different error zones and converging factors are depicted in Fig. 7. As shown in Fig. 7(a), the nonlinear PD controllers with $\alpha \in (0,\ 1)$ produce higher force than the linear PD controller, in which the error is located at the interval with $|e| \le \delta$ except the set points. In practical applications, a higher force can eliminate errors effectively and is better for position and speed tracking. When large error appears with $|e| > \delta$ in Fig. 7(b), selecting $\alpha \in (1,\ \infty)$ is appropriate to generate higher force, which allows the suspension part to converge to the original point and stabilize the system. Therefore, the nonlinear PD controller provides higher force than the linear PD controller. It reduces the response time of small vibration and suppresses large oscillation.

For the proposed nonlinear PD controller in this paper, the converging factor is selected as $\alpha \in (0,\ 1)$ with small error and $\alpha \in (1,\ \infty)$ with large error. The parameters of nonlinear PD are listed in Table IV. It can be concluded that the time-varying nonlinear gains are greater than the linear gains in most cases, i.e.,

$$k_{np} \ge k_{lp}, \quad k_{nd} \ge k_{ld}. \tag{16}$$

*2) Stability of Nonlinear PD Controller:* The Popov stability criterion provides sufficient stability judgment for time-varying nonlinear controlled system. The transfer function of the controlled active suspension model can be expressed as

$$W(s) = G(s)(k_{np} + k_{nd}s) = \frac{\frac{1}{M_s}(k_{np} + k_{nd}s)}{s^2 + \frac{C_s}{M_s}s + \frac{K_s}{M_s}} \tag{17}$$

where $G(s) = (1/(M_s))/s^2 + (C_s/M_s)s + (K_s/M_s)$ is the transfer function of the suspension system model.

By applying the Popov criterion, the time-varying nonlinear gains are chosen to make sure that the Popov plot lies entirely to the right of a straight line with nonnegative slope and intersect

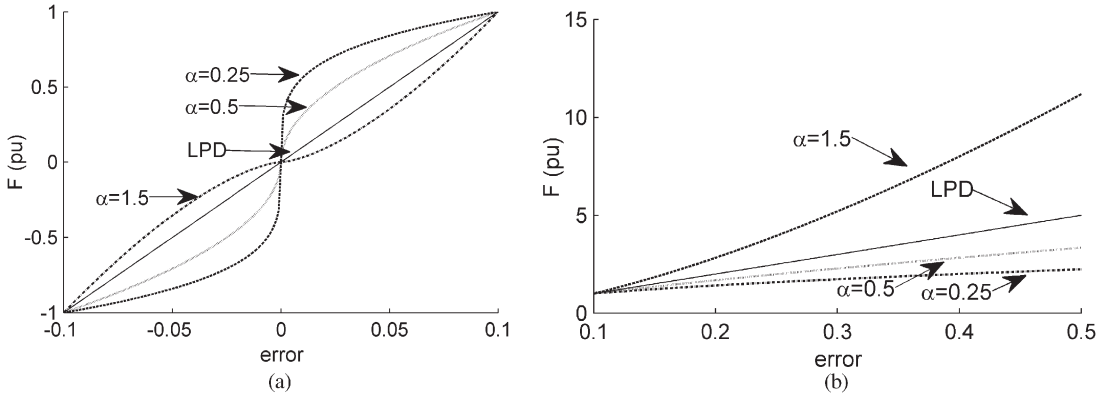


Fig. 7. Comparison between the outputs of linear and nonlinear PD controllers. (a) Small error. (b) Large error.

the negative real axis [25]. As discussed in [17], [19], the Popov plot can be divided into two cases: 1) $C_s k_{np} \geq K_s k_{nd}$ and 2) $C_s k_{np} < K_s k_{nd}$. The stability of the nonlinear PD controlled system for both cases can be guaranteed by $k_{np} > 0$ and $k_{nd} > 0$.

*3) Robustness Analysis:* The robustness analysis of the linear PD controller and the nonlinear PD controller discussed here is divided into two parts: 1) parameters variation, and 2) external disturbance. The frequently varied parameter of the active suspension system is the sprung mass. From (17), the variation of sprung mass changes the poles of the controlled system; the effects of parameter variation are almost the same on both controlled system. Moreover, the system parameters are positive all the time. The Popov plots of the controlled systems lie entirely to the right side of the straight line; therefore, both systems are always stable.

When the external bounded disturbances are injected, the input errors are nonzero, and some bounded gains exist to represent the disturbance as follows:

$$d_u = \frac{K_s}{M_s} z_u + \frac{C_s}{M_s} \dot{z}_u \triangleq g_1(\cdot) z_s + g_2(\cdot) \dot{z}_s = -g_1(\cdot) e_p - g_2(\cdot) e_d \tag{18}$$

where $g_1(\cdot)$ and $g_2(\cdot)$ are bounded nonlinear time-varying terms related to external bounded disturbances. When external disturbances occur, the active suspension system vibrates, and then $e_p$ and $e_d$ are not equal to zero. Hence, nonzero $g_1(\cdot)$ and $g_2(\cdot)$ exist for (18). Furthermore, it is reasonable to say that large terms appear when large disturbances are injected.

The general transfer function with equivalent external disturbance (18) is

$$W_r(s) = \frac{\frac{1}{M_s}(k_{pr} + k_{dr} s)}{s^2 + \frac{C_s}{M_s} s + \frac{K_s}{M_s}} \tag{19}$$

where $k_{lpr} \equiv k_{pr} = k_{lp} - g_1$ and $k_{ldr} \equiv k_{dr} = k_{ld} - g_2$ for the linear PD controller, and $k_{npr} \equiv k_{pr} = k_{np} - g_1$ $k_{ndr} \equiv k_{dr} = k_{nd} - g_2$ for the nonlinear PD controller.

From (16) and (19), the following inequality always exists: $k_{npr} \geq k_{lpr}$, and $k_{ndr} \geq k_{ldr}$. When the disturbances are small, particularly within the set-point errors, the controller gains of both controllers are large enough to keep the system stable. As the disturbances increase, if $g_1$ and $g_2$ increase as well, the control gains $k_{npr}$, $k_{ndr}$, $k_{lpr}$, and $k_{ldr}$ decrease eventually. Once the external disturbances exceed the tipping point, $k_{lpr}$ and/or $k_{ldr}$ decrease to minus negative, whereas $k_{npr}$ and $k_{ndr}$ still remain positive. Based on the Popov stability criterion, the linear PD controller has negative gains, and the Popov plot lies into the left side of the straight line. The controlled system becomes unstable. Meanwhile, the nonlinear PD controller lies entirely in the right side of the straight line, and the controlled system is therefore stable. Therefore, the nonlinear PD controller is more robust than the linear PD controller with regard to the variation of external disturbances.

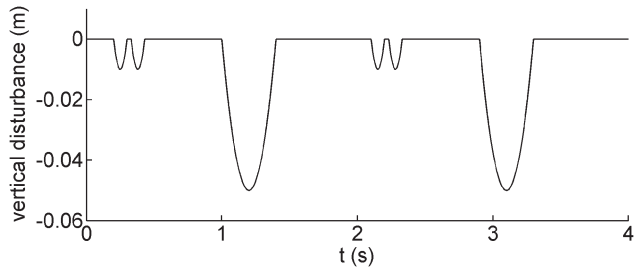


Fig. 8. Road profile of test rig.

TABLE III
PARAMETER OF ACTIVE SUSPENSION SYSTEM

| Symbol | Value |
|---|---|
| $M_s$ | 110 kg |
| $M_u$ | 90 kg |
| $K_s$ | 18600 N/m |
| $K_u$ | 160000 N/m |
| $C_s$ | 600 N/(m/s) |

## IV. SIMULATION AND EXPERIMENT RESULTS

A test rig of the quarter-car active suspension system based on TMS320F2808 fix-point DSP was built at the laboratory, as shown in Fig. 2. The road model of the test rig is a rolling wheel with concave plates. Hence, the road profile is a periodical surface with three isolated bumps described in Fig. 8. The system parameters are specified in Table III. The parameters of the TD and PD controllers are tuned through simulation and listed in Table IV.

Suppose that the car is running on a road similar to the test rig. The output force of the LSRA is restricted within

TABLE IV
PARAMETER OF CONTROLLER

| Symbol | Value | Symbol | Value |
|---|---|---|---|
| $v$ | 200 | $\alpha_{p1}$ | 2 |
| $c$ | 10 | $\alpha_{p2}$ | 0.5 |
| $h$ | 0.00025 | $\delta_p$ | 0.01 |
| $K_{lp}$ | 30000 | $\alpha_{d1}$ | 1.5 |
| $K_{ld}$ | 3200 | $\alpha_{d2}$ | 0.75 |
| $K_{np}$ | 250 | $\delta_d$ | 0.1 |
| $K_{nd}$ | 200 | | |

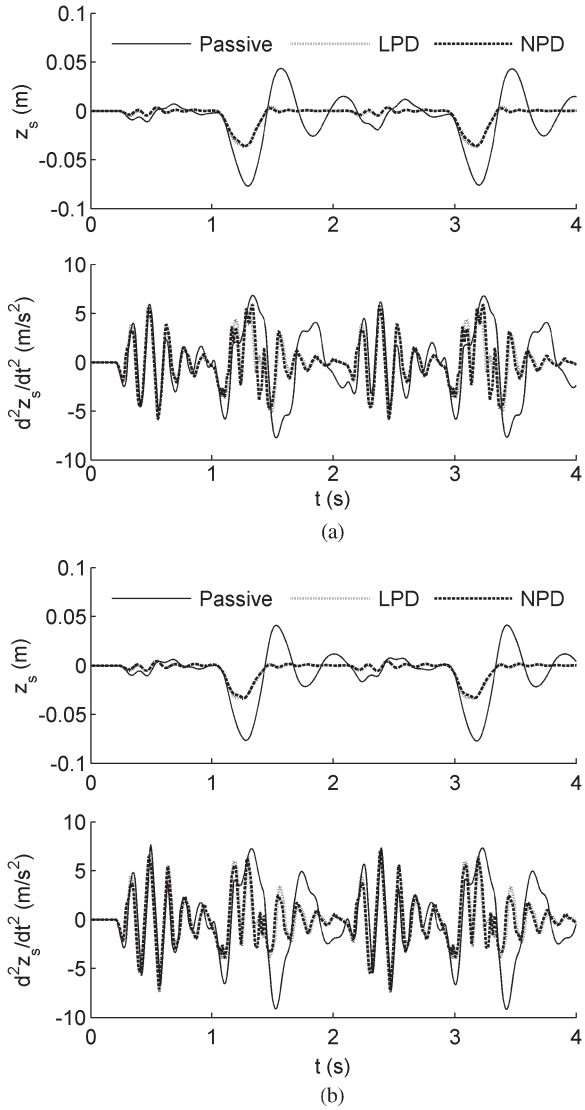


Fig. 9. Comparison of passive and active suspension system with variation of sprung mass and actuator force restriction. (a) $M_s = M_{s0}$. (b) $M_s = 80\% M_{s0}$.

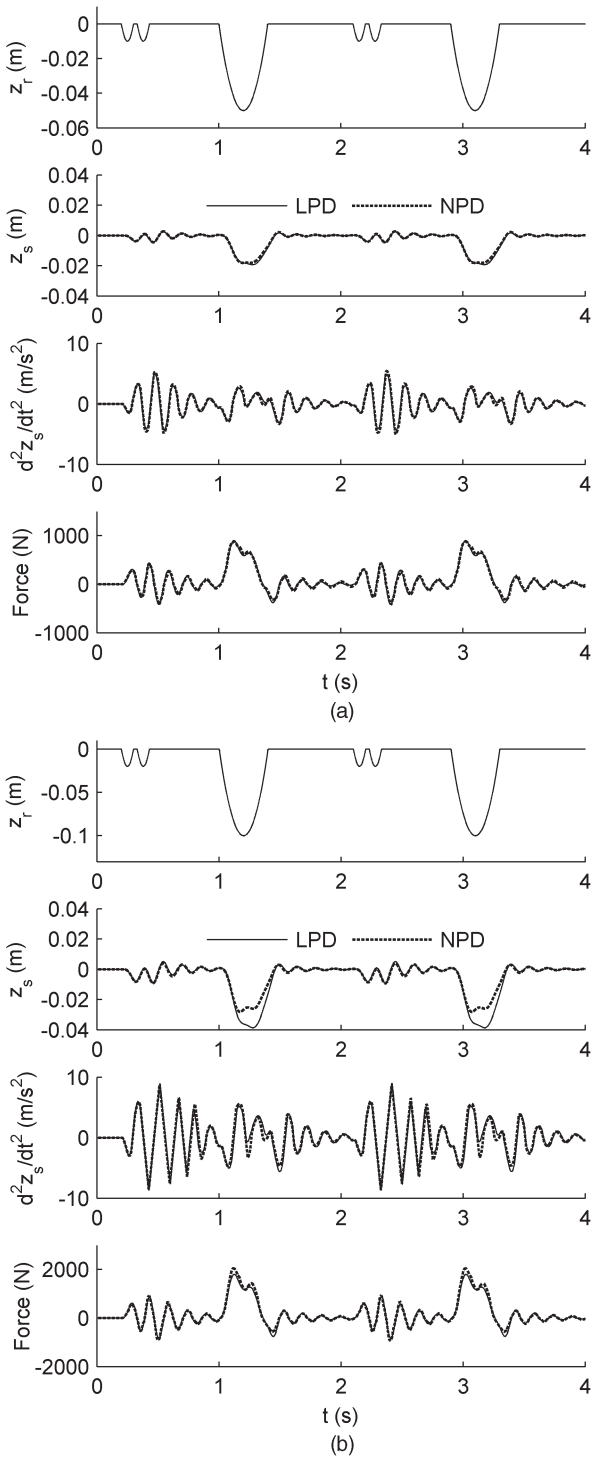


Fig. 10. Response of active suspension with different road inputs. (a) Road disturbance with nominal amplitude. (b) Road disturbance with two times nominal amplitude.

[−900, 900] due to the mechanical limitation and protection of the whole system. Examinations of robustness are simulated with the variation of sprung mass and external disturbance, as shown in Figs. 9 and 10. The responses of the passive and active suspension system are figured out first when the sprung mass varies from 80% to 100% of its nominal value. The vertical displacement and acceleration of the sprung mass subsystem are suppressed significantly with PD controllers, which indicate that the performance of the active suspension system is better than the passive suspensions system. Moreover, the responses of the linear and nonlinear PD controllers are almost the same on both cases. The results show that the sprung mass variations have the same effects on both controllers, as previously discussed.

The robustness of PD controllers related to road disturbances is verified in Fig. 10. The road profile amplitude is assumed to be deepened to twice of the original road terrain. In Fig. 10(a),

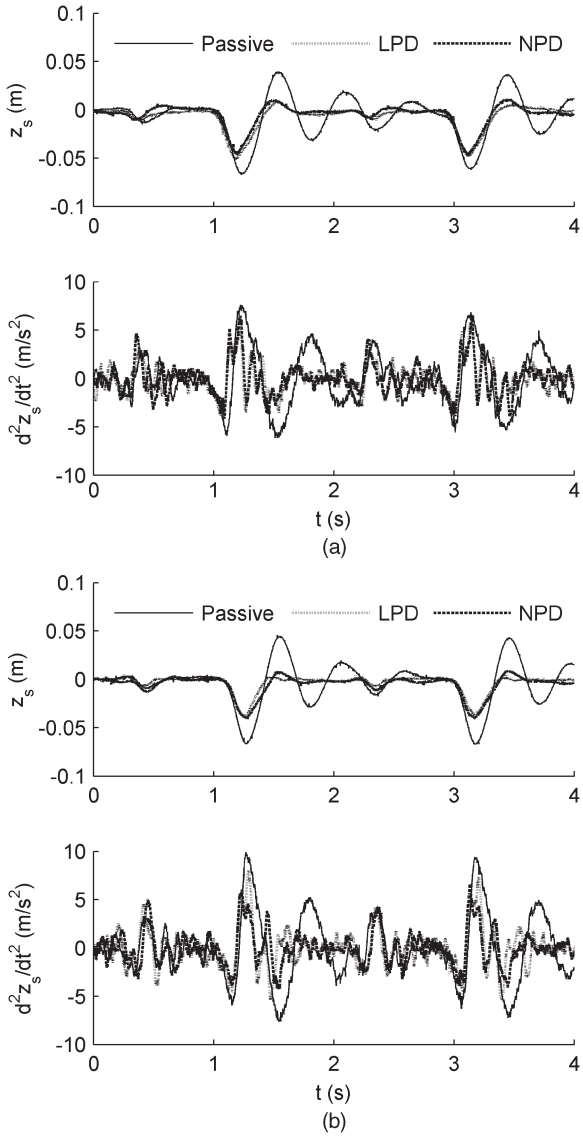


Fig. 11. Experiment results of active suspension system with varied sprung mass. (a) $M_s = M_{s0}$. (b) $M_s = 80\% M_{s0}$.

both control methods are stable, and the displacement converges to zero quickly. When the disturbance increases twice, the equivalent control gains will be decreased, as discussed in (19). It can be seen that the equivalent control gains of the linear PD in (19) are closer to zero than the gains of the nonlinear PD controller. Hence, the performance of the controlled system with linear PD will be deteriorated dramatically. Fig. 10(b) shows that the displacement of the system using the nonlinear PD controller is reduced significantly compared with the linear PD controller due to the higher generated peak force. It is verified that the nonlinear PD controller is more robust than the linear PD controller when the external disturbance increases dramatically.

To verify the effectiveness of the linear PD controller and the proposed nonlinear PD controller, experiments are conducted with a variety of sprung masses. It is obvious that active suspension systems are more effective than passive suspension systems according to the experiment results shown in Fig. 11, and both the displacement and the acceleration of sprung mass are reduced significantly. From the experimental results shown in Fig. 11, a minor deviation between the linear PD controller and the proposed nonlinear PD controller is observed, which cannot be observed in the simulation results shown in Fig. 9. One of the possible reasons to that incoherence is the limitation and accuracy in computation of the DSP. The nonlinear PD controller deals with more floating-point calculations, and hence, a compromise has to be made between data accuracy and range, which result in the produced force difference between simulation and experiment occasionally. Other possible reasons are the estimation error of parameters, such as the equivalent damper coefficient and the difference of force characteristics of LSRA between FEA data and practical force.

In Fig. 11(a), the maximum accelerations of active suspension and passive suspension are almost the same under the deepest hole, which is due to the restriction of peak force provided by the LSRA. To reduce the maximum acceleration, the peak output force value of the LSRA should be increased to suppress the dynamic oscillation significantly.

## V. Conclusion

A novel active electromagnetic suspension system adopting LSRA has been presented in this paper. The developed linear actuator is simple and reliable and offers a favorable alternative in low-cost high-performance linear propulsion application. TD is introduced to calculate the velocity directly from vertical displacement and reject the sensor noise effectively, which is unavailable in conventional calculation. PD control methods, both linear and nonlinear cases, are studied and designed to achieve the required dynamic performance while maintaining its simplicity and robustness, which is suitable for real-time application. A thorough comparison between linear PD control and nonlinear PD control has been made. Simulation and experiment results have demonstrated the effectiveness of the active suspension system with LSRA adopting the two control methods. Moreover, the proposed nonlinear PD control method enhances the robustness of the active suspension system and is more suitable in complicated road terrain than the linear PD controller.

The force characteristic of LSRA is altered with position and current and is also affected by saturation effect. To enhance the force control accuracy, the nonlinearity of the LSRA should be studied, and a compensation method will be proposed to achieve precise control.

## Appendix

For a given reference signal $r(t)$, the purpose of TD is to obtain its tracking signal $r_1(t) = r(t)$ and derivative $r_2(t) = \dot{r}(t)$. Two lemmas and Theorem 1 are presented here. The proof can be referred to [17] and [24].

*Lemma 1:* For a continuous function $z(t)$, where $t \geq 0$ satisfies $\lim_{t\to\infty} z(t) = 0$, if $w(t) = z(\Omega t)$, $\Omega > 0$ exists, then the equation $\lim_{\Omega\to\infty} \int_0^T |w(t)|dt = 0, \forall T > 0$ is valid.

*Lemma 2:* If the solutions to the system

$$\begin{cases} \dot{z}_1 = z_2 \\ \dot{z}_2 = f(z_1,\ z_2) \end{cases} \tag{A1}$$

satisfy that $z_1(t) \to 0$ and $z_2(t) \to 0$ as $t \to \infty$, then for an arbitrarily constant $c$ and $T > 0$, the solution $w_1(t)$ to the following system

$$\begin{cases} \dot{w}_1 = w_2 \\ \dot{w}_2 = \Omega^2 f(w_1 - c,\ w_2/\Omega) \end{cases} \tag{A2}$$

meets

$$\lim_{\Omega \to \infty} \int_0^T |w_1(t) - c|\, dt = 0. \tag{A3}$$

The proof of Lemmas 1 and 2 based on the mean value theorem and the associated Theorem 1 [17], [24] are described below.

*Theorem 1:* If arbitrary solutions to the system, as shown in (A1), satisfy $z_1(t) \to 0$ and $z_2(t) \to 0$ as $t \to \infty$, then for any arbitrarily bounded integrable function $r(t)$ and given constant $T > 0$, the solution $r_1(t)$ to the system

$$\begin{cases} \dot{r}_1 = r_2 \\ \dot{r}_2 = \Omega^2 f(r_1 - r,\ r_2/\Omega) \end{cases} \tag{A4}$$

satisfies

$$\lim_{\Omega \to \infty} \int_0^T |r_1(t) - r(t)|\, dt = 0. \tag{A5}$$

Theorem 1 shows that for a bounded integrable function $r(t)$, $r_1(t)$ on average converges to $r(t)$ following the TD, and $r_2(t)$ weakly converges to the generalized derivative of $r(t)$.

## REFERENCES


[1] I. Martins, J. Esteves, G. D. Marques, and F. P. da Silva, "Permanent-magnets linear actuators applicability in automobile active suspensions," *IEEE Trans. Veh. Technol.*, vol. 55, no. 1, pp. 86–94, Jan. 2006.

[2] J. T. Broch, *Mechanical Vibration and Shock Measurements*. Nærum, Denmark: Brüel & Kjær, 1984.

[3] B. L. J. Gysen, J. L. G. Janssen, J. J. H. Paulides, and E. A. Lomonova, "Design aspects of an active electromagnetic suspension system for automotive applications," *IEEE Trans. Ind. Appl.*, vol. 45, no. 5, pp. 1589–1597, Sep./Oct. 2009.

[4] S. Lee and W. J. Kim, "Active suspension control with direct-drive tubular linear brushless permanent-magnet motor," *IEEE Trans. Control Syst. Technol.*, vol. 18, no. 4, pp. 859–870, Jul. 2010.

[5] R. Krishnan, *Switched Reluctance Motor Drives: Modeling, Simulation, Analysis, Design, and Applications*. Boca Raton, FL: CRC Press, Jun. 2001.

[6] H. S. Lim, R. Krishnan, and N. S. Lobo, "Design and control of a linear propulsion system for an elevator using linear switched reluctance motor drives," *IEEE Trans. Ind. Electron.*, vol. 55, no. 2, pp. 534–542, Feb. 2008.

[7] S. W. Zhao, N. C. Cheung, W.-C. Gan, and J. M. Yang, "High-precision position control of a linear-switched reluctance motor using a self-tuning regulator," *IEEE Trans. Power Electron.*, vol. 25, no. 11, pp. 2820–2827, Nov. 2010.

[8] Z. G. Sun, N. C. Cheung, S. W. Zhao, and W.-C. Gan, "Magnetic analysis of switched reluctance actuators in levitated linear transporters," *IEEE Trans. Veh. Technol.*, vol. 59, no. 9, pp. 4280–4288, Nov. 2010.

[9] N. S. Lobo, H. S. Lim, and R. Krishnan, "Comparison of linear switched reluctance machines for vertical propulsion application: Analysis, design, and experimental correlation," *IEEE Trans. Ind. Appl.*, vol. 44, no. 4, pp. 1134–1142, Jul./Aug. 2008.

[10] H. Hannoun, M. Hilairet, and C. Marchand, "Design of an SRM speed control strategy for a wide range of operating speeds," *IEEE Trans. Ind. Electron.*, vol. 57, no. 9, pp. 2911–2921, Sep. 2010.

[11] J. Cao, H. Liu, P. Li, and D. J. Brown, "State of the art in vehicle active suspension adaptive control systems based on intelligent methodologies," *IEEE Trans. Intell. Transp. Syst.*, vol. 9, no. 3, pp. 392–405, Sep. 2008.

[12] N. Yagiz, Y. Hacioglu, and Y. Taskin, "Fuzzy sliding-mode control of active suspensions," *IEEE Trans. Ind. Electron.*, vol. 5, no. 11, pp. 3883–3890, Nov. 2008.

[13] H. Li, H. Liu, H. Gao, and P. Shi, "Reliable fuzzy control for active suspension systems with actuator delay and fault," *IEEE Trans. Fuzzy Syst.*, vol. 20, no. 2, pp. 342–357, Apr. 2012.

[14] J. Lin and R.-J. Lian, "Intelligent control of active suspension systems," *IEEE Trans. Ind. Electron.*, vol. 58, no. 2, pp. 618–628, Feb. 2011.

[15] H. Gao, W. Sun, and P. Shi, "Robust sampled- data H$\infty$ control for vehicle active suspension systems," *IEEE Trans. Control Syst. Technol.*, vol. 18, no. 1, pp. 238–245, Jan. 2010.

[16] K. J. Åström and T. Hägglund, *PID Controllers—Theory, Design, and Tuning*, 2nd ed. Lisboa, Portugal: ISA Press, 1995.

[17] Y. X. Su, D. Sun, and B. Y. Duan, "Design of an enhanced nonlinear PID controller," *Mechatronics*, vol. 15, no. 8, pp. 1005–1024, Oct. 2005.

[18] H. Seraji, "A new class of nonlinear PID controllers with robotic applications," *J. Robot Syst.*, vol. 15, no. 3, pp. 161–181, 1998.

[19] J. Han, "From PID to active disturbance rejection control," *IEEE Trans. Ind. Electron.*, vol. 56, no. 3, pp. 900–906, Mar. 2009.

[20] X. D. Xue, K. W. E. Cheng, and S. L. Ho, "A self-training numerical method to calculate the magnetic characteristics for switched reluctance motor drives," *IEEE Trans. Magn.*, vol. 40, no. 2, pp. 734–737, Mar. 2004.

[21] X. D. Xue, K. W. E. Cheng, and S. L. Ho, "Trigonometry-based numerical method to compute nonlinear magnetic characteristics in switched reluctance motors," *IEEE Trans. Magn.*, vol. 43, no. 4, pp. 1845–1848, Apr. 2007.

[22] X. D. Xue, K. W. E. Cheng, and S. L. Ho, "Online and offline rotary regression analysis of torque estimator for switched reluctance motor drives," *IEEE Trans. Energy Convers.*, vol. 22, no. 4, pp. 810–818, Dec. 2007.

[23] Z. Zhang, N. C. Cheung, K. W. E. Cheng, X. D. Xue, and J. K. Lin, "Direct instantaneous force control with improved efficiency for four-quadrant operation of linear switched reluctance actuator in active suspension system," *IEEE Trans. Veh. Technol.*, vol. 61, no. 4, pp. 1567–1576, May 2012.

[24] J. Q. Han and W. Wang, "Nonlinear tracking-differentiator," *J. Syst. Sci. Math. Sci.*, vol. 14, no. 2, pp. 177–183, 1994.

[25] P. C. Parks and V. Hahn, *Stability Theory*. New York: Prentice-Hall, 1993.


**Jiongkang Lin** received the B.Eng. degree from Huazhong University of Science and Technology, Wuhan, China, in 2003 and the M.Eng. degree from South China University of Technology, Guangzhou, China, in 2007. He is currently working toward the Ph.D. degree with the Department of Electrical Engineering, The Hong Kong Polytechnic University, Kowloon, Hong Kong.

He has been a Research Assistant with the Department of Electrical Engineering, The Hong Kong Polytechnic University. His research interests include motion control and power electronics.

**Ka Wai Eric Cheng** (M'90–SM'06) received the B.Sc. and Ph.D. degrees from the University of Bath, Bath, U.K., in 1987 and 1990, respectively.

He was a Principal Engineer with Lucas Aerospace, U.K., where he led a number of power electronics projects before he joined The Hong Kong Polytechnic University, Kowloon, Hong Kong, in 1997, where he is currently a Professor and the Director of the Power Electronics Research Centre. He has authored over 300 published papers and seven books. His research interests include power electronics, motor drives, electromagnetic interference, electric vehicles, and energy saving.

Prof. Cheng received the Institution of Electrical Engineers Sebastian Z. De Ferranti Premium Award in 1995, the Outstanding Consultancy Award in 2000, the Faculty Merit Award for Best Teaching in 2003 from The Hong Kong Polytechnic University, the Faculty Engineering Industrial and Engineering Services Grant Achievement Award in 2006, the Brussels Innova Energy Gold Medal With Mention in 2007, the Consumer Product Design Award in 2008, the Electric Vehicle Team Faculty Merit Award of the university in 2009, and Geneva's Invention Expo Silver medal for vehicle solar air-conditioning in 2011.

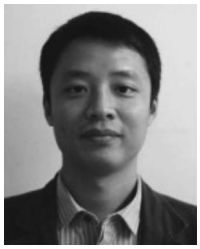

**Zhu Zhang** (S'11) received the M.Eng, degree from South China University of Technology, Guangzhou, China, in 2004 and the Ph.D. degree from The Hong Kong Polytechnic University, Kowloon, Hong Kong, in 2012.

He is currently a Research Associate with the Department of Electrical Engineering, The Hong Kong Polytechnic University. His research interests include electrical machines, electrical drives, and power electronics.

**Norbert C. Cheung** (S'85–M'91–SM'05) received the B.Sc. degree from the University of London, London, U.K., in 1981, the M.Sc. degree from the University of Hong Kong, Kowloon, Hong Kong, in 1987, and the Ph.D. degree from the University of New South Wales, Kensington, NSW, Australia, in 1996.

He was a Technical Manager with ASM Assembly Automation Ltd., Hong Kong, for two years, working in the areas of intelligent motion control and robotics systems. Since 1997, he has been with The Hong Kong Polytechnic University, where he is currently with the Department of Electrical Engineering.

Dr. Cheung is a Chartered Engineer in the U.K. and a member of the Institution of Engineering and Technology, U.K.

**Xiangdang Xue** (M'10) received the B.Eng. degree from Hefei University of Technology, Hefei, Anhui, China, in 1984, the M.Eng. degree from Tianjin University, Tianjin, China, in 1987, and the Ph.D. degree from The Hong Kong Polytechnic University, Hong Kong, in 2004, all in electrical engineering.

From 1987 to 2001, he was a Lecturer and an Associate Professor engaged in teaching and research with the Department of Electrical Engineering, Tianjin University. He is currently a Research Fellow with the Department of Electrical Engineering, The Hong Kong Polytechnic University. He has published over 90 papers. His research interests are in the areas of electrical machines, electrical drives, and power electronics. His current research is focused on electric machines, electric actuators, and electrical drives applied to electric vehicles.

**Tsz Wang Ng** received the M.Sc. degree from the University of Hong Kong, Kowloon, Hong Kong, in 2009.

He is currently a Research Associate with the Department of Electrical Engineering, The Hong Kong Polytechnic University, Kowloon. His research interests include charging stations, power electronics, and finite-element analysis.